Effective-medium theory of surfaces and metasurfaces containing two-dimensional binary inclusions

A. Alexopoulos*

Electronic Warfare and Radar Division, Defence Science and Technology Organisation (DSTO), P.O. Box 1500, Edinburgh, South Australia 5111, Australia

(Received 26 November 2009; revised manuscript received 3 February 2010; published 29 April 2010)

The paper extends one-body effective-medium theory to incorporate the correct second-order interactions in a two-dimensional Maxwell-Garnett theory. The two-body inclusion problem is solved using the averaged dipole moments that are induced by the scattering electromagnetic field on the medium/inclusion system. By incorporating the appropriate polarizability factor in the solutions, conventional right-handed media with binary embeddings are analyzed while a different form for the polarizability term allows the study of the effective properties of a metasurface. In both cases, it is shown that the two-body coefficient to second order in the low area fraction of inclusions is exact, while the corresponding results of the Maxwell-Garnett and Bruggeman theories are incorrect. This is especially true in the superconducting and holes limits, respectively. In the study of metasurfaces, the requirement for electromagnetic screening of the inclusions as well as the requirement needed to achieve the Fröhlich condition are stated. Negative permittivity and permeability are presented for strong-scattering showing negative resonances for a given frequency spectrum. It is shown that these resonances disappear when we derive the weak-scattering limit. The possibility of obtaining doubly negative effective permittivity and permeability is discussed by using an appropriate polarization for the applied electromagnetic field propagating in the metasurface. Finally, the potential difference and hence voltage and capacitance between binary inclusions is determined for surfaces/metasurfaces which allows, in the case of metasurfaces, the behavior of split-ring-type resonators to be investigated.

DOI: 10.1103/PhysRevE.81.046607 PACS number(s): 41.20.−q, 77.84.Lf

I. INTRODUCTION

The construction of technological devices relies heavily on the understanding of the physical properties of material structures. Inhomogeneous media with inclusions in them have been associated with the discovery of materials with performance characteristics ranging from electrostatic/magnetostatic behavior, heat conduction, or diffusion to elasticity and porosity effects to name a few. The properties of such composite media are studied via macroscopic averaging of inclusion-medium interactions which are utilized to obtain effective parameters. In recent years, based on the original ideas of Veselago [1], left-handed composite systems have been researched for their remarkable performance properties [2–11]. Just as in the case of right-handed media, negative index media require the derivation of effective parameters which underpin general metamaterial design. One interesting approach to such metamaterials is to consider a set of inclusions placed in a two-dimensional (2D) pattern at a surface or interface whose scattering characteristics achieve some desired effective electric and/or magnetic response. Such specialized metamaterial structures have been given the specific name of metasurfaces or metafilms. Metasurfaces have the advantage of being less lossy compared to bulk metamaterial structures while there has been much interest in using them for the design of smart surfaces involving such areas as scattering cancellation, cavity resonators, waveguide structures, and antenna element design. In this paper we will investigate some of the effective properties of surfaces containing inclusions and consider other effects that might prove useful for the general understanding of surface/metasurface structures. The approach taken is to show that for a suitable polarization factor γ, both right-handed and left-handed media with embeddings in them can be incorporated in the one approach and using effective-medium theory (EMT) various parameters of interest can be derived. In what follows later, we see that this is achieved by making use of a two-layer inclusion model that also allows an analysis of split-ring-type resonating structures (SRRs) [12]. While EMT is by no means the only theory one can make use of, it is nevertheless the most successful and versatile approach for the study of many physical systems. The central concept of EMT is very simple: it describes how one inclusion interacts with the surrounding host medium. The interactions are then averaged over the entire medium containing n inclusions. The solution to this one-body problem is an old one and requires knowledge of the local field $\mathbf{E}_{local}$ in the vicinity of the inclusion. In 1870 Lorentz [13] investigated this issue while he was developing his ideas of macroscopic electrodynamics. However, Lorentz's results did not describe a microscopic field nor the average field of the medium, and for this reason his theory received much criticism [14]. What was required in order to improve the ideas of Lorentz was a proper connection between microscopic and macroscopic parameters. One promising method is to relate the dipole moment of an inclusion to the local field. This approach has resulted in the familiar Clausius-Mossotti equations which work well for various dielectric liquids and gases. The difficulty of the Clausius-Mossotti equations has always been the correct representation of the polarizability γ since the latter was obtained by semiclassical models as

*aris.alexopoulos@dsto.defence.gov.au

opposed to quantum-mechanical formulations. Extensions to the Clausius-Mossotti theory have been made which have resulted in the Maxwell-Garnett (MG) theory. The MG approach has been extended by Bruggeman who has studied symmetry effects in two-phase composite systems among other things. The Maxwell-Garnett and Bruggeman theories are correct to first order but fail when we consider second-order effects. In order to fully understand the properties of surfaces and metasurfaces, these second-order effects have to be incorporated in a conventional EMT which is something that we consider in Sec. III. The approach taken is to determine the total dipole moments between binary inclusions which are induced by the external electromagnetic field using the method of images which has been studied extensively by many over the years from as far back as when it was founded by Thomson [15]. It is well known that the effective permittivity and permeability of materials/metamaterials are determined as a virial expansion in the volume fraction of inclusions c (later on, because we are dealing with 2D, c will be referred to as the area fraction of inclusions). In the case of right-handed materials the exact $O(c)$ coefficient for a spherical inclusion was obtained by Maxwell in 1873 [16] while the second-order coefficient of $O(c^2)$ took more than 100 years to be solved due to its complexity. In particular Djordjević *et al.* [17] used complicated hyperbolic recurrence relations to obtain a slowly convergent series of hundreds of terms for this coefficient for two-dimensional inclusions. In Secs. III and IV we examine extensions to EMT in order to correctly account for binary interactions between inclusions with cylindrical geometry in a random distribution and show that modification of the polarizability factor in the Maxwell-Garnett equation can be used in the design of doubly negative effective permittivity and permeability metasurfaces. In the appropriate limit, the polarizability factor also yields permittivity and permeability results for a conventional right-handed surface.

II. MODIFIED EFFECTIVE-MEDIUM THEORY

There are many theoretical models that are commonly used in order to describe the effective properties of a medium with inclusions embedded in it. One approach is due to Bruggeman's symmetric and asymmetric formulation but, like some mean-field theories, neglects correlations. On the other hand, Bruggeman's symmetric theory makes nontrivial predictions of percolation. Another method based on the Clausius-Mossotti equation is the Maxwell-Garnett theory that for most applications shows good results. Both of these EMTs have the same underlying principle: that is, they are one-body theories that describe the interaction of one inclusion with the host medium. This one-body interaction is averaged throughout the medium to obtain the effective parameters of the composite. The problem with these EMT theories is that when two-body interactions are included they inevitably fail. In the case of Bruggeman the maximum error is 100% while for the MG theory the maximum error is 50%, corresponding to the perfect-conducting limits [18]. In the Maxwell-Garnett theory, the effective permittivity $\bar{\epsilon}$ for a medium containing two-dimensional inclusions with permittivity ϵ_1 is given by

$$\frac{\bar{\epsilon}-\epsilon_0}{\bar{\epsilon}+\epsilon_0}=c\left(\frac{\epsilon_1-\epsilon_0}{\epsilon_1+\epsilon_0}\right) \tag{1}$$

where ϵ_0 is the permittivity of the host medium and c is the area fraction of inclusions. Equation (1) can be written as

$$\frac{\bar{\epsilon}}{\epsilon_0}=1+\frac{2\gamma c}{1-\gamma c} \tag{2}$$

where we define $\gamma \equiv \gamma_{MG}$,

$$\gamma_{MG}=\frac{\epsilon_1-\epsilon_0}{\epsilon_1+\epsilon_0}\equiv\frac{\frac{\epsilon_1}{\epsilon_0}-1}{\frac{\epsilon_1}{\epsilon_0}+1} \tag{3}$$

which is proportional to the polarizability and arises from the Maxwell-Garnett one-body EMT. For density distributions where the area fraction of inclusions c is low Eq. (2) becomes

$$\frac{\bar{\epsilon}}{\epsilon_0}=1+2\gamma_{MG}c+2\gamma_{MG}^2c^2+\cdots. \tag{4}$$

Equation (4) is the virial expansion for the permittivity $\bar{\epsilon}$ in terms of the area fraction of inclusions c to second order. The coefficient of c in Eq. (4) is exact because this is just Maxwell's description of one-body interactions with the medium and is what is described by conventional effective-medium theory. However the theory does not account correctly for the two-body interactions as represented by the coefficient of c^2, i.e., $2\gamma_{GM}^2$. This term is highly erroneous in its present form so what is needed is a proper development of binary-inclusion interactions that improve dramatically the results of conventional EMT up to second order in c. Incorporating these second-order corrections is vital for the accurate design and understanding of surface/metasurface structures. To highlight this notion we examine the validity of Eq. (4) for the perfect-conducting limit where $\epsilon_1/\epsilon_0\to\infty$ which implies from Eq. (3) that $\gamma_{MG}=1$. Equation (4) now becomes

$$\frac{\bar{\epsilon}}{\epsilon_0}=1+2c+2c^2+O(c^3) \tag{5}$$

which shows that the second-order coefficient is wrong because as we will show later, the correct expansion should be

$$\frac{\bar{\epsilon}}{\epsilon_0}=1+2c+2.7449c^2+O(c^3) \tag{6}$$

also in agreement with the result obtained by others in this limit [17]. It is worth also mentioning that Bruggeman's theory is even worse giving this term as $4c^2$. From the virial expansion for $\bar{\epsilon}$ we can see $O(c^3)$ terms appearing in the series, and it can be surmised that these higher orders in c represent many-body interactions; e.g., the coefficient of c^3 would require the solution of the three-body problem and this is mathematically intractable to say the least. In what follows we will only be concerned with the determination of the (relative) permittivity $\epsilon=\bar{\epsilon}/\epsilon_0$ to second order by determining κ in the expansion

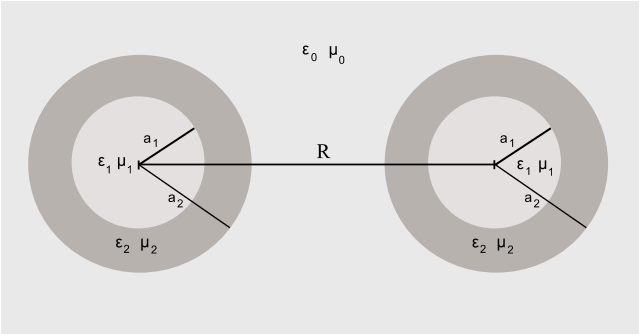

FIG. 1. (Color online) Double-layered nonoverlapping inclusions in a plane with parameters and radii defined. One inclusion only interacting with the medium is described by conventional EMT which is a first-order interaction theory. We consider two inclusions (a binary pair as shown) interacting with each other as well as the medium thus modifying EMT to a second-order interaction theory.

$$\epsilon = 1 + 2\left(\frac{\epsilon_1 - \epsilon_0}{\epsilon_1 + \epsilon_0}\right)c + \kappa c^2 \tag{7}$$

where ϵ here is for a one-layer inclusion and will allow us to investigate *right-handed composite* surfaces. Furthermore the same mathematical form as Eq. (7) can be used to determine the permeability μ,

$$\mu = 1 + 2\left(\frac{\mu_1 - \mu_0}{\mu_1 + \mu_0}\right)c + \lambda c^2 \tag{8}$$

where λ represents the two-body interactions in the medium with effective permeability μ. Thus we can determine ϵ or μ using the same approach as discussed in Sec. III. Notice that the coefficient of c in Eqs. (7) and (8) is proportional to the Maxwell-Garnett polarizability factor γ_{MG} and is valid to first order for normal right-handed composite systems. In order to investigate metasurfaces or to model split-ring resonator-type inclusions embedded in them, Eqs. (7) and (8) are modified to include a two-layered inclusion system with inner and outer layers defined in Fig. 1. Modifying Eqs. (7) and (8) for metasurfaces we obtain

$$\epsilon = 1 + \kappa c^2 + 2\left[\frac{(\gamma_1 - 1)(\gamma_2 + 1) + \beta(\gamma_2 - 1)(\gamma_1 + 1)}{(\gamma_1 + 1)(\gamma_2 + 1) + \beta(\gamma_1 - 1)(\gamma_2 - 1)}\right]c \tag{9}$$

where we define $\gamma_1 = \epsilon_2/\epsilon_0$, $\gamma_2 = \epsilon_1/\epsilon_2$. Similarly for the permeability we have

$$\mu = 1 + \lambda c^2 + 2\left[\frac{(\gamma_1 - 1)(\gamma_2 + 1) + \beta(\gamma_2 - 1)(\gamma_1 + 1)}{(\gamma_1 + 1)(\gamma_2 + 1) + \beta(\gamma_1 - 1)(\gamma_2 - 1)}\right]c \tag{10}$$

with $\gamma_1 = \mu_2/\mu_0$, $\gamma_2 = \mu_1/\mu_2$. In Eqs. (9) and (10) c is the area fraction of inclusions and $\beta = a_1^2/a_2^2$ is the fraction of the area occupied by the inner layer of a two-layer inclusion as opposed to the total area of the inclusion. Equations (9) and (10) are general forms that can be used to model the behavior of left-handed and right-handed media utilizing parametric quantities as given in Fig. 1. We can see this because if we let $\epsilon_1 = \epsilon_2$ or $\mu_1 = \mu_2$, $\beta = 1$ and set $\epsilon_2 \equiv \epsilon_1$ or $\mu_2 \equiv \mu_1$, Eqs. (9) and (10) reduce to Eqs. (7) and (8). It is now a matter of determining the second-order contributions κ and λ.

III. DETERMINATION OF THE SECOND-ORDER INTERACTIONS κ AND λ

One approach that can be used to determine the second-order interactions κ and λ is via the use of bipolar coordinates, but this is not a trivial undertaking. Conformal mapping techniques have been successful but are limited to the perfect-conducting limit. This limit has been studied in quite some detail [19,20] for right-handed composite systems. In what follows we will make use of the method of images because it more easily facilitates the analysis of two-body interactions. We consider our pair of inclusions with radius a_2 (for the two-layer version, see Fig. 1) with their respective centers separated by the distance R. Moreover there are two cases where the external electromagnetic field is incident on the medium and inclusions, namely, the perpendicular and parallel directions which induce an infinite set of dipole moments. The position of the dipoles is determined via a continued fraction representation. The approach is based on the method of images which is a well-known technique in classical field theory. For this reason we will not dwell on the details here but suffice to say that a more detailed account can be found in [19] for example. The total dipole moment for the binary inclusions is given as a combination of the parallel contributions due to the dipoles being in alignment with the field and the perpendicular contributions which are equal in magnitude to the parallel case but with alternating sign. Once we have all the dipole moments to the n^{th} order that are aligned and perpendicular to the external field, it is a matter of obtaining the polarizability which is proportional to κc^2 and λc^2, terms that will be explained in detail later. As we shall see, the polarizability is determined by averaging the parallel and perpendicular dipole moments of the binary inclusions and integrating over the entire medium. In Sec. III A we derive the dipole moments for the two-body problem.

A. Field-induced dipole moments

When an electromagnetic field is incident on a medium of permittivity ϵ_0 and permeability μ_0, respectively, the field influences the interaction of the embedded inclusions and the medium itself. Specifically the electric-field component $\mathbf{E}_0$ induces dipole-dipole interactions between the binary inclusions; i.e., it induces dipole moments consisting of dipole and image dipole pairs. Since the inclusions are symmetric we can determine the dipole moments of the first inclusion interacting with the second, since the interactions of the second inclusion with the first are the same. Thus for the inclusion on the left say, see Fig. 1, and considering the presence of the inclusion to the right, the field creates a dipole p_1 at the center of inclusion 1 and an image dipole p_2 created in the inclusion on the right. This in turn creates a dipole image in the inclusion to the left namely p_3 and so on until an

infinite set is created. Proceeding in the same way but starting from the right inclusion we once again obtain the same infinite set of dipoles moments. Overall, in the end both inclusions contain the same number of images whose positions are given by b_n (see below). The perpendicular field case gives the same distribution of dipole moments as the parallel case except in alternating directions with each successive iteration. The first dipole moment at the center of inclusion 1 on the left is written as

$$p_1 = 2\pi a_2^2 E_0 \left[\frac{(\gamma_1 - 1)(\gamma_2 + 1) + \beta(\gamma_2 - 1)(\gamma_1 + 1)}{(\gamma_1 + 1)(\gamma_2 + 1) + \beta(\gamma_1 - 1)(\gamma_2 - 1)} \right] \tag{11}$$

where $\gamma_1 = \epsilon_2/\epsilon_0$, $\gamma_2 = \epsilon_1/\epsilon_2$, and $\beta = a_1^2/a_2^2$. Let the subsequent position of each dipole moment be given by the continued fraction

$$b_k = \frac{a_2^2}{R - b_{k-1}}. \tag{12}$$

We define the parameter γ to be

$$\gamma = \frac{(\gamma_1 - 1)(\gamma_2 + 1) + \beta(\gamma_2 - 1)(\gamma_1 + 1)}{(\gamma_1 + 1)(\gamma_2 + 1) + \beta(\gamma_1 - 1)(\gamma_2 - 1)} \tag{13}$$

then the second dipole moment is created at $b_1 = a_2^2/R$ with $b_0 = 0$,

$$p_2 = 2\pi a_2^2 E_0 \gamma^2 \left(\frac{a_2}{R} \right)^2. \tag{14}$$

The mathematical complexity of the dipole moments increases with higher orders as can be seen with the third-order contribution which is displaced at position b_2 and it becomes

$$p_3 = 2\pi a_2^2 E_0 \gamma^3 \left(\frac{a_2}{R} \right)^2 \left(\frac{a_2}{R - \frac{a_2^2}{R}} \right)^2 \tag{15}$$

and so on, where R is the separation of the two inclusion centers. To obtain the right convergence the number of dipole moments that are necessary tends to infinity especially as the two inclusions approach each other (closely packed) or in the limit where they touch. By defining $b_k = a_2 \omega_k$ we can replace all b_k by the transformation,

$$\omega_k = \frac{\omega}{1 - \omega \omega_{k-1}} \tag{16}$$

where $\omega_1 \equiv \omega = a_2/R$, $\omega_0 = 0$, and γ is given by Eq. (13). Generalizing Eqs. (14) and (15) we obtain the n^{th}-order dipole contributions due to the parallel component of the field $\mathbf{E}_0$ as

$$p_n^{\parallel} = 2\pi a_2^2 E_0 \gamma^n \prod_{k=1}^{n-1} \omega_k^2. \tag{17}$$

Furthermore, the field in the perpendicular direction induces dipoles moments that differ from the parallel case only in sign so that

$$p_n^{\perp} = 2(-1)^{n-1} \pi a_2^2 E_0 \gamma^n \prod_{k=1}^{n-1} \omega_k^2. \tag{18}$$

From Eqs. (17) and (18) we can now write down the *total* preaveraged dipole moment $p_n \equiv p_n^{\parallel} + p_n^{\perp}$,

$$p_n = 2\pi a_2^2 E_0 (1 + (-1)^{n-1}) \gamma^n \prod_{k=1}^{n-1} \omega_k^2. \tag{19}$$

Equation (19) is the n^{th}-order total dipole moment which, as we shall see below, will be used to determine the second-order coefficient κ or λ, i.e., the two-body interactions which conventional EMT in its present form lacks. From Eq. (13) we can investigate the condition that is needed for "cloaking" the inclusions. This requires that $\gamma = 0$ so that the effective permittivity is $\bar{\epsilon} = \epsilon_0$ or $\epsilon = 1$. To achieve this we set the numerator of Eq. (13) to zero and solve for γ_2,

$$\gamma_2 = \left[1 - \frac{1}{\beta} \left(\frac{\gamma_1 - 1}{\gamma_1 + 1} \right) \right] \Big/ \left[1 + \frac{1}{\beta} \left(\frac{\gamma_1 - 1}{\gamma_1 + 1} \right) \right] \tag{20}$$

and from the definition of γ_1 and γ_2 this is written as

$$\epsilon_1 = \epsilon_2 \frac{\epsilon_2 + \epsilon_0 - (\epsilon_2 - \epsilon_0)/\beta}{\epsilon_2 + \epsilon_0 + (\epsilon_2 - \epsilon_0)/\beta} \tag{21}$$

whereby given the outer layer permittivity ϵ_2, for example, and ϵ_0, the required permittivity for the inner layer ϵ_1 that makes the inclusion invisible is determined. The approach above is also valid if instead of permittivities we used effective permeability μ with corresponding parameters μ_1, μ_2, and μ_0. It is interesting to note that by setting the denominator of Eq. (13) to zero instead would lead to the familiar Fröhlich condition that is very important in the study of resonance effects in small particles, e.g., surface excitations. It is also important in the determination of the radar scattering cross section of disk-shaped targets that depend on the ratio A/λ^2, where A is the area of a disk and λ is the wavelength. Determination of the total dipole interactions between the two inclusions in the medium now allows us to define the second-order coefficients as being

$$\kappa = \lambda = 2 \left[\gamma^2 + \sum_{n=1}^{\infty} F_{2n+1}(\gamma) \right]. \tag{22}$$

Hence the expansion for the permittivity and permeability to second order in the low area fraction of inclusions can now be expressed as

$$\epsilon = 1 + 2\gamma c + 2 \left[\gamma^2 + \sum_{n=1}^{\infty} F_{2n+1}(\gamma) \right] c^2 + O(c^3) \tag{23}$$

and

$$\mu = 1 + 2\gamma c + 2 \left[\gamma^2 + \sum_{n=1}^{\infty} F_{2n+1}(\gamma) \right] c^2 + O(c^3), \tag{24}$$

respectively, where $F(\gamma)$ is averaged and integrated over the entire medium via the use of the total dipole moments obtained before

$$F_n(\gamma) = \frac{1}{2\pi a_2^4 E_0} \int_{2a_2}^{\infty} (p_n^{\parallel} + p_n^{\perp}) R dR. \tag{25}$$

From Eq. (19) and making the transformation to ω via $\omega = a_2/R$ Eq. (25) finally becomes

$$F_n(\gamma) = [1 + (-1)^{n-1}]\gamma^n \int_0^{1/2} \frac{1}{\omega} \left[\prod_{k=2}^{n-1} \omega_k^2 \right] d\omega \tag{26}$$

where once again ω_k is obtained from Eq. (16) and γ is given by Eq. (13). We note that from Eq. (22) the sum is infinite, and this in itself would be a major obstacle in the determination of κ and λ. However in reality the series can be truncated to N which is relatively small in order depending on the desired precision. Even so, later we will consider how the binary inclusions interact at close range (even touching) when we look at the potential difference (voltage) between them. This requires that for convergence to be maintained, the number of interacting terms that need to be considered must be large, i.e., $N \to \infty$.

B. Surface composites

To investigate the effective parameters of a right-handed binary system require that we consider a one-layer inclusion model. This implies reducing γ given by Eq. (13) to the form

$$\gamma = \frac{\gamma_1 - 1}{\gamma_1 + 1} \tag{27}$$

that for reasons mentioned before, we set $\gamma_1 = \epsilon_1/\epsilon_0$ or $\gamma_1 = \mu_1/\mu_0$. The effective permittivity of the medium is now determined from

$$\epsilon = 1 + 2\left(\frac{\gamma_1 - 1}{\gamma_1 + 1}\right) c + \kappa c^2 \tag{28}$$

and similarly for the effective permeability we have

$$\mu = 1 + 2\left(\frac{\gamma_1 - 1}{\gamma_1 + 1}\right) c + \lambda c^2, \tag{29}$$

respectively. The second-order binary interactions κ and λ are determined via Eq. (22), and so

$$\kappa \equiv \lambda = 2\left(\frac{\gamma_1 - 1}{\gamma_1 + 1}\right)^2 + 4\sum_{n=1}^{N} \left\{ \left(\frac{\gamma_1 - 1}{\gamma_1 + 1}\right)^{2n+1} \int_0^{1/2} \frac{1}{\omega} \left[\prod_{k=2}^{2n} \omega_k^2 \right] d\omega \right\}. \tag{30}$$

Notice that Eq. (30) has been obtained via Eq. (26) for odd n since even values of n imply that $F_n(\gamma) = 0$. Using these results we consider two important limits of interest: (i) the perfect-conducting limit where $\epsilon_1/\epsilon_0 \to \infty$ $(\mu_1/\mu_0 \to \infty)$ and (ii) the "holes" limit where $\epsilon_1/\epsilon_0 \to 0$ $(\mu_1/\mu_0 \to 0)$. In Table I we show convergence for κ (or λ) which is superior to and in agreement with the value obtained by Djordjević *et al.* [17] who use over 100 terms in a complicated hyperbolic series expansion to obtain this limit. In Table II we show the "holes" limit where the effective properties of the composite are due mostly from the dominating permittivity (permeability) of the host medium rather than those of the inclusions. Figure 2 is a plot of the two-body interaction terms κ and λ appearing to second order in the area fraction of inclusions for the permittivity and permeability, respectively, against the inclusion permittivity $\epsilon_{1,2}$ and permeability $\mu_{1,2}$. The solid curve represents the results derived in this paper while the short-dashed curve is due to the Maxwell-Garnett theory. The importance of correctly calculating the second-order terms is emphasized here with the Maxwell-Garnett result giving the wrong distribution. Interestingly, for the perfect-conducting limit at the value "3" shown, the predicted convergence in this paper gives the value 2.744 90 (see Table I) while the Maxwell-Garnett theory gives the value "2." Compare with Eqs. (5) and (6) in Sec. II. In the "holes" limit at "−3" the value converges to 1.256 19 (see Table II) while the Maxwell-Garnett theory predicts the value "2." Apart from the strong-scattering solution, as shown in Fig. 2, there is also a corresponding weak-scattering solution. To determine the weak-scattering approximation we consider the limit $\epsilon_1/\epsilon_0 \to 1$ so that

TABLE I. Shown are values for κ or λ using n^{th}-order dipole images in the perfect-conducting limit, that is, when $\gamma = 1$ or $\epsilon_1/\epsilon_0 \to \infty$ and $\mu_1/\mu_0 \to \infty$. Here n is the order in $F_n(\gamma)$, or Eq. (26). Values of up to $n = 37$ are determined. Known value: $\kappa = 2.744\,989\ldots$ from [17].

n	κ_n or λ_n	n	κ_n or λ_n
3	2.66667	21	2.74454
5	2.72234	23	2.74464
7	2.73551	25	2.74471
9	2.74015	27	2.74477
11	2.74219	29	2.74481
13	2.74323	31	2.74484
15	2.74381	33	2.74487
17	2.74416	35	2.74488
19	2.74439	37	2.74490

TABLE II. Shown are values of κ or λ using n^{th}-order dipole images in the "holes" limit, that is, when $\gamma = -1$ or $\epsilon_1/\epsilon_0 \to 0$ and $\mu_1/\mu_0 \to 0$. Here n is the order in $F_n(\gamma)$, or Eq. (26). Values of up to $n = 15$ are enough to obtain very good convergence.

n	κ_n or λ_n
3	1.33333
5	1.27766
7	1.26449
9	1.25985
11	1.25780
13	1.25677
15	1.25619

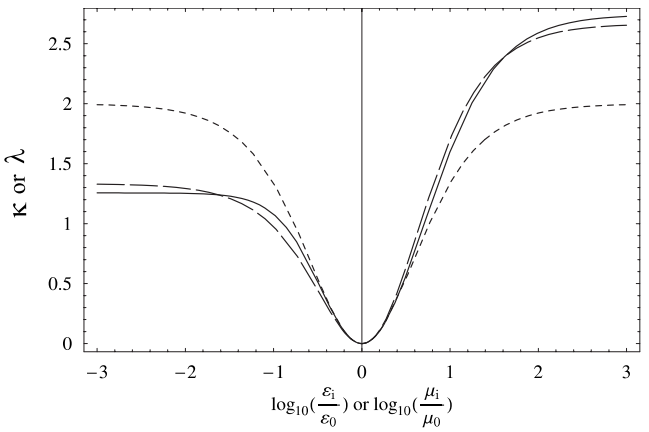

FIG. 2. The two-body interaction terms κ and λ appearing to second order in the area fraction of inclusions for the permittivity and permeability, respectively, are shown as a function of the inclusion permittivity ϵ_i and permeability μ_i where $i=1,2$ represents inclusion 1 or 2. The solid curve represents the results derived in this paper while the short-dashed curve is due to the Maxwell-Garnett theory. The long-dashed curve which is close to the solid curve is the weak-scattering approximation.

$$\kappa = 2\gamma^2 + 4\gamma^3 \int_0^{1/2} \frac{\omega}{(1-\omega^2)^2} d\omega = 2\left(\frac{\epsilon_1 - \epsilon_0}{\epsilon_1 + \epsilon_0}\right)^2 + \frac{2}{3}\left(\frac{\epsilon_1 - \epsilon_0}{\epsilon_1 + \epsilon_0}\right)^3 \tag{31}$$

and likewise $\mu_1/\mu_0 \to 1$, and so

$$\lambda = 2\left(\frac{\mu_1 - \mu_0}{\mu_1 + \mu_0}\right)^2 + \frac{2}{3}\left(\frac{\mu_1 - \mu_0}{\mu_1 + \mu_0}\right)^3. \tag{32}$$

The weak-scattering limit is shown in Fig. 2 where a comparison with the strong-scattering (solid) curve is made. The effective permittivity ϵ and permeability μ are shown in Fig. 3 as a function of the inclusion permittivity ϵ_1 and permeability μ_1 against the area fraction of inclusions c. In what follows we examine metasurface behavior.

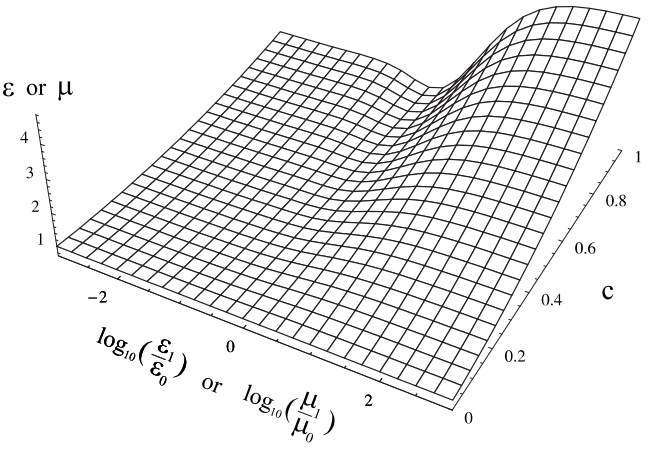

FIG. 3. The effective permittivity ϵ or permeability μ to second order as a function of the inclusion to medium permittivity (permeability) ratio ϵ_1/ϵ_0 (μ_1/μ_0) and area fraction of inclusions c.

C. Metasurface composites

There are two requirements which are essential in the construction of left-handed materials or more precisely negative refractive index materials. First, the permittivity ϵ has to be negative and this is relatively easy to accomplish. In fact negative values for permittivity can also be obtained for normal right-handed materials which we have looked at in Sec. III B. In the case of metamaterials, for example, $\epsilon<0$ is obtained by distributing thin cylindrical wires inside the medium. The second much more difficult requirement is to obtain a negative permeability μ which together with the negative permittivity produce the properties of a metamaterial. One successful approach for obtaining negative μ is via the use of SRRs that typically consist of a pair of concentric annular rings with terminations (splits) at opposite ends. A magnetic field incident on the rings induces rotating currents which cause the rings to emit their own flux that either enhances or opposes the incident field depending on the SRRs resonant properties. The rings are constructed with a small gap between them which creates a large capacitance that lowers the resonant frequency (we consider this effect in Sec. IV when we look at the voltage between the inclusion pair). Below resonant frequency the real part of the magnetic permeability of the SRR becomes positively large but for frequencies higher than the resonating frequency the permeability becomes negative. In this section we consider these concepts and investigate what the design parameters must be in order to obtain negative and doubly negative ϵ and μ for two-dimensional inclusions embedded in a metasurface. Since SRRs are embedded in a medium and consist of rings, we note that these are analogous to our two-dimensional inclusions with double layers (rings) embedded in a metasurface. We are interested in how the parameters resembling those of SRRs and rods can be modeled in an effective-medium approach which allows the determination of the effective properties and behavior of metasurfaces. The permittivity ϵ and permeability μ of a metasurface to second order in the area fraction of inclusions is given as

$$\epsilon = \mu = 1 + 2\gamma c + \left\{ 2\gamma^2 + 4\sum_{n=1}^{N} \left[\gamma^{2n+1} \int_0^{1/2} \frac{1}{\omega} \left[\prod_{k=2}^{2n} \omega_k^2 \right] d\omega \right] \right\} c^2 \tag{33}$$

where according to Fig. 1 for the two-layer inclusions we have

$$\gamma = \frac{(\gamma_1 - 1)(\gamma_2 + 1) + \beta(\gamma_2 - 1)(\gamma_1 + 1)}{(\gamma_1 + 1)(\gamma_2 + 1) + \beta(\gamma_1 - 1)(\gamma_2 - 1)}. \tag{34}$$

The required behavior of the metasurface is now dictated by the appropriate choice of the filling fraction β and the permittivities and permeabilities of the medium and the inclusion inner and outer layers. In our approach it is seen that the necessary condition for the realization of negative ϵ/μ requires that the inclusion layers have at least opposite signs in the permittivity/permeability, assuming that the host medium has a positive value for both of these. This is demonstrated in Fig. 4 where, for given γ_1 values, a plot of the

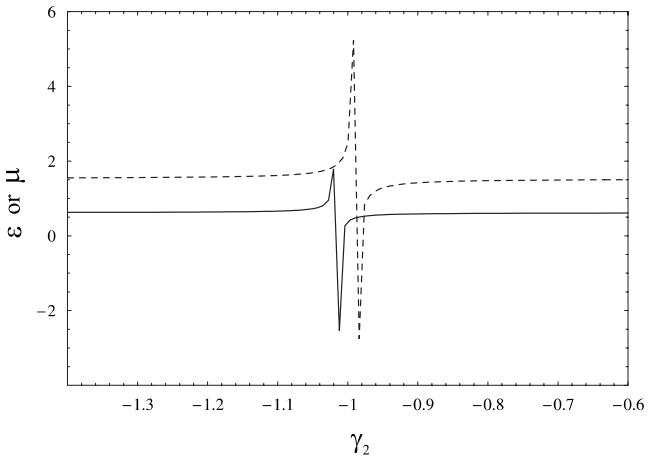

FIG. 4. Plot shows that at least γ_2 must be a negative ratio in order to achieve effective ϵ or μ that is negative. Results are shown for two different values of γ_1. Parameters used are: $\gamma_1=0.13$ (solid); $\gamma_1=5.5$ (dashed); and $c=0.3$ and $\beta=(0.1)^2$.

effective ϵ, μ is made as a function of γ_2, thus indicating that $\gamma_2<0$ is required for the metasurface to have a negative effective response in this design. A general problem of interest is the case where the permittivity/permeability of the outer and inner layers of the inclusions are functions of frequency. Suppose that the outer layer is made up of a metallic substance which has a permittivity as a function of frequency as described by the Drude model. Then,

$$\epsilon_2 = 1 - \frac{f_p^2}{f^2 + \alpha f i} \tag{35}$$

where for free electrons or plasmons in a metal f_p is the plasma frequency and α is the damping constant. On the other hand let us assume that the inner layer is made up of a magnetic material that is also frequency dependent so that in this case the permeability μ_1 is given by [21]

$$\mu_1 = 1 - \frac{f^2}{f^2 - f_m^2 + \bar{\alpha} f i} \tag{36}$$

where now f_m is the magnetic resonance and $\bar{\alpha}$ is again the damping constant. In the practical sense, the implementation of such a Lorentzian response is achieved via resonators such as split rings or other alternative methods [22]. Then by optimizing the parameters in this design it is possible to obtain negative permittivity/permeability values so that the effective-medium properties correspond to those of a metasurface. In Fig. 5 we show the case where there is strong interaction between the pair of inclusions and the host medium for an area fraction of inclusions value of $c=0.1$, filling fraction $\beta=0.64$, $\epsilon_0=2.0$, $\epsilon_1=4.0$, $f_p=5.55$, $\alpha=0.7$, $\mu_0=2.0$, $\mu_2=3.0$, $f_m=4.0$, and $\bar{\alpha}=0.59$. In the strong-scattering limit the interaction between the inclusions is greater, i.e., as N in Eq. (33) increases, so the result is the manifestation of resonances with negative values at different regions of the frequency spectrum. In contrast, for the weak-scattering limit, also discussed in Sec. III B for normal right-handed composites, the resonances are reduced as can be seen in Fig. 6,

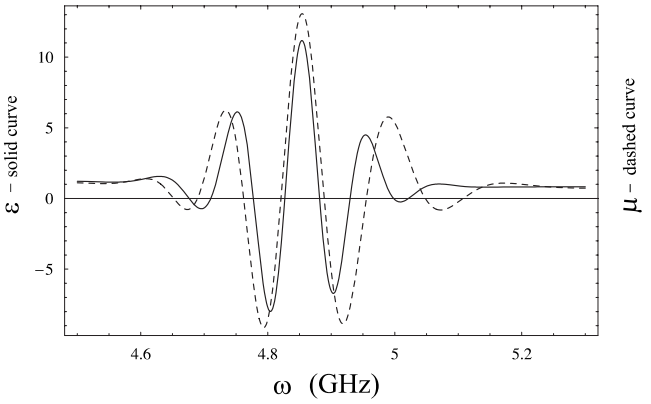

FIG. 5. Strong-scattering negative effective resonances (bandwidths) for the permittivity ϵ and permeability μ of a metasurface via second-order corrections to standard EMT.

where we take here $c=0.1$, $\beta=0.64$, $\epsilon_0=2.0$, $\epsilon_1=4.0$, $f_p=5.45$, $\alpha=0.18$, $\mu_0=2.0$, $\mu_2=3.0$, $f_m=4.0$, and $\bar{\alpha}=0.15$. Note that in Figs. 5 and 6 both ϵ_2 and μ_1 have negative permittivity and permeability, respectively, for the frequency range concerned. We now consider obtaining a doubly negative effective response (DNG) for a metasurface using the binary inclusions as shown in Fig. 1. The requirement is that we excite an electric response from the outer layer and a magnetic response from the inner layer of the inclusions, respectively, as the electromagnetic field propagates along the metasurface. One approach is to consider dielectric relaxation and magnetic hysteresis or more generally polarization hysteresis, but we could instead make use of pulses of electromagnetic waves with alternating polarization so that the required layers in the inclusions are excited by the correct component of the field. Even so, we are hampered by the fact that at very high frequencies in particular, the permeability has zero effect rendering any contributions from magnetic dipoles essentially nonexistent. Thus the importance of electric and magnetic dipoles and whether there is strong coupling between them depends on the frequency according to the Landau-Lifshitz theory. Hence it is important to examine the validity of frequency-dependent doubly negative permittivity and permeability for very high frequencies in particular

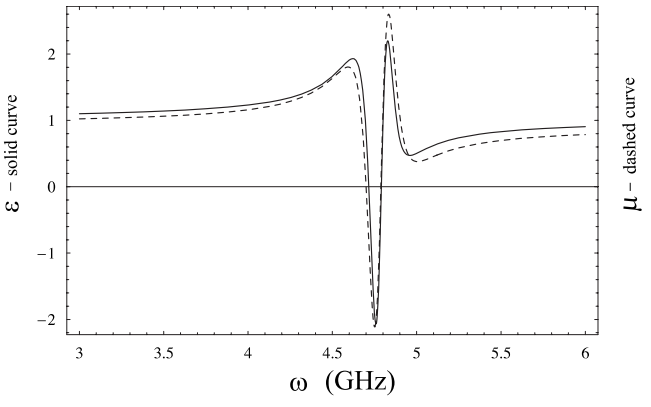

FIG. 6. Weak-scattering negative effective permittivity ϵ and permeability μ of a metasurface via second-order corrections to standard EMT.

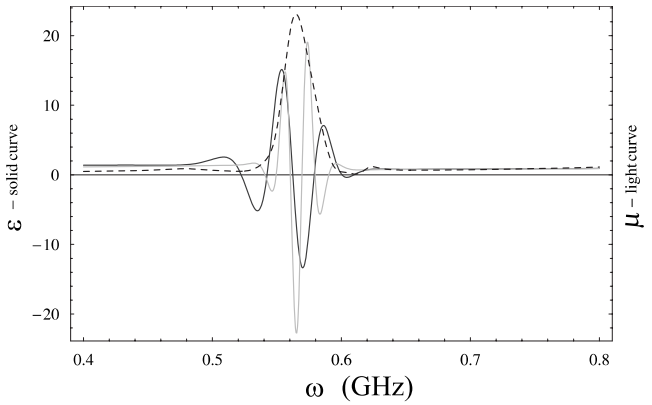

FIG. 7. Doubly negative effective permittivity ϵ (solid curve) and permeability μ (light curve) is shown for a metasurface containing binary inclusions. While the resonant behavior generally indicates that there are regions where DNG may be possible over different frequency bands, the reality is that the Agranovich-Gartstein criterion restricts such behavior to a very narrow band as shown by the dashed curve, i.e., at approximately ω=0.56 GHz for the parameters chosen.

[23–26]. Concerning the permeability, Landau and Lifshitz [23] stated that it ceases to have any physical significance for very high frequencies, and if this is true then doubly negative results are certainly in doubt. However, composite media with artificial structures in them do not necessarily fall into this category and should not be in opposition to the Landau-Lifshitz theory. In fact as Agranovich and Gartstein (AG) [27] pointed out, at sufficiently high frequencies the permeability can lose its relationship to the total induced magnetic moment and magnetically induced currents cannot be considered as a separate issue; however, the situation can be resolved for small frequencies. In other words, the induced magnetic moment is the sum of the magnetization (analogous to the polarization) and the time-dependent dielectric polarization. The latter is negligible for certain frequencies whereby the magnetization dominates. The condition that meets the latter requirement is given by what we shall term as the AG [27] criterion $R(\omega)$ involving the permittivity $\epsilon(\omega)$ and permeability $\mu(\omega)$,

$$R(\omega) = \left| \frac{\epsilon(\omega)(\mu(\omega) - 1)}{\epsilon(\omega) - 1} \right| \gg 1. \tag{37}$$

As the frequency increases particularly in the optical range, criterion (37) implies that the effect of the purely magnetic response is very small. On the other hand Eq. (37) is satisfied when the frequency becomes small so that the magnetic currents and the permeability become tangible. The AG criterion (dashed curve) is calculated for the doubly negative results in Fig. 7 which shows that the greater the value is, the more plausible the doubly negative results are. Unfortunately as can be seen, this criterion restricts the frequency range to small values and the range in which DNG results hold is very restricted which is perhaps one of the reasons why doubly negative metamaterials have narrow-band performance. Here the parameters considered are: c=0.1, β=0.81, ϵ_0=2.33, ϵ_1=4.0, f_p=4.49, α=0.122, μ_0=1.0, μ_2=6.9, f_m=0.45, and $\bar{\alpha}$=0.0415. Finally, it is possible to select parameters in such a way as to make it appear that the medium does not contain any inclusions when in reality it does and the conditions that make this possible are given by Eqs. (20) and (21). It is worth noting that various limits can be taken for γ in Eq. (34) via γ_1, γ_2, and β that can be used in the design specifications of a metasurface including the perfect-conducting limit for example with results being exactly the same as for a normal right-handed surface (see Table I).

IV. POTENTIAL DIFFERENCE BETWEEN THE BINARY INCLUSIONS

The problem of finding the potential difference or voltage and hence capacitance between inclusions has been a topic of great interest when it comes to the understanding of general composite materials and metamaterials. Most of the results deal with the one-body medium interaction because of the complexity involved. Nevertheless attempts have been made to study pair interactions particularly for spherical inclusions that are independent of any medium. Calculations have been made of the capacity of touching unequal metallic spheres, while studies have also been made for nontouching spheres under a variety of conditions. In addition to calculations of capacity and the total charge between two spheres and the electrostatic force, consideration has been made for dielectric sphere pairs in uniform external fields using a Green's-function technique for difference equations. Asymptotic solutions for separated conducting spheres and touching dielectric spheres have been proposed. For two-dimensional pair inclusions in a medium the voltage has been obtained using complex asymptotic expansions of hyperbolic functions. In most of the cases mentioned above the results involve field expansions in curvilinear coordinates such as bispherical coordinates. In essence, most of the field expansion techniques require an infinite matrix equation which must be truncated and inverted numerically to obtain the multipole moments. When the inclusions are close to touching the number of multipole moments that need to be retained for an accurate solution makes numerical inversion impractical. What is required is a method for calculating the influence exerted between nearest-neighbor inclusions explicitly, that is without numerical inversion, thus providing an estimate of the induced multipoles to all orders which among other things would simplify the calculation of the effective properties of closely packed surfaces/metasurfaces. The approach we have considered in Secs. II and III will be used to circumvent the problems and complexities associated with field expansion methods in order to investigate the behavior of pair inclusions in metasurfaces. In addition, as the pair-inclusions approach each other, the number of dipole moments required in order to maintain convergence is enormous and in the limit where they touch becomes infinite. Fortunately we will derive an expression that allows the determination of the voltage (capacitance) between the inclusions for this limit without the need for all the dipole moment contributions. We consider the two-inclusion model (with inner and outer layers analogous to split-ring resonators) in the presence of an electromagnetic field. In particular, using the electric-field

component $\mathbf{E}_0$ (with a similar argument for the magnetic field component), the potential difference or voltage existing between the two inclusions is

$$\Delta V = E_0 R + 2\sum_{n=2}^{\infty} V_n \tag{38}$$

where factor "2" appearing in Eq. (38) accounts for the effect of both inclusions due to symmetry. The contribution V_n from the dipole moments is

$$V_n = -\frac{1}{2\pi a_2^2} b_{n-1} p_{n-1} \tag{39}$$

where recall that the dipole image displacements are given by

$$b_n = \frac{a_2^2}{R - b_{n-1}}. \tag{40}$$

Once again defining $b_n = a_2 \omega_n$, Eq. (38) becomes

$$\frac{\Delta V}{V_0} = \frac{R}{a_2} - \frac{1}{\pi a_2 V_0} \sum_{n=2}^{\infty} \omega_{n-1} p_{n-1} \tag{41}$$

where $V_0 = a_2 E_0$. From the definition of the dipole moments derived previously we can replace p_n. The potential difference (voltage) between two binary inclusions interacting with the medium is now given by

$$\frac{\Delta V}{V_0} = \frac{R}{a_2} - 2\left[\left(\frac{a_2}{R}\right)\gamma + \sum_{n=2}^{\infty} \omega_n \gamma^n \left(\prod_{k=1}^{n-1} \omega_k^2\right)\right]. \tag{42}$$

Equation (42) gives the voltage and hence capacitance C since

$$C = \frac{Q}{\Delta V} \tag{43}$$

for metasurfaces, where Q is the total charge and γ is

$$\gamma = \frac{(\gamma_1 - 1)(\gamma_2 + 1) + \beta(\gamma_2 - 1)(\gamma_1 + 1)}{(\gamma_1 + 1)(\gamma_2 + 1) + \beta(\gamma_1 - 1)(\gamma_2 - 1)}. \tag{44}$$

Recall that for the case of right-handed surface composites we have

$$\gamma = \frac{\epsilon_1 - \epsilon_0}{\epsilon_1 + \epsilon_0} \equiv \gamma_{MG} \tag{45}$$

if we reduce γ from a two-layer inclusion to a one-layer inclusion. From a detailed study of the behavior of the continued fraction

$$\omega_n = \frac{\omega}{1 - \omega\omega_{n-1}}, \tag{46}$$

we find that when the two inclusions touch at $R/a_2 = 2$, Eq. (46) reduces to the simple form

$$\omega_n = \frac{n}{n+1}. \tag{47}$$

Hence, in the limit where the inclusions touch we determine the voltage as being

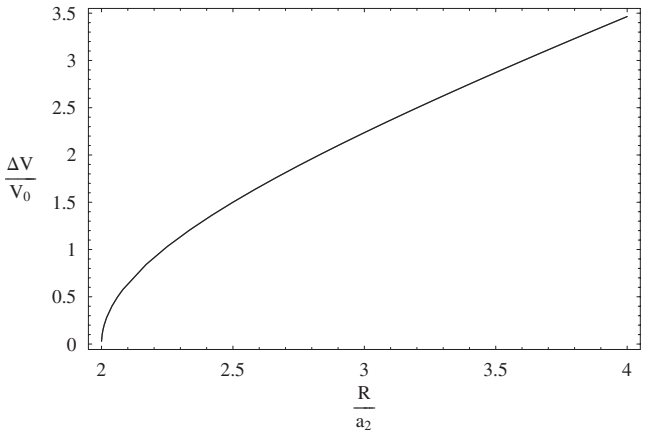

FIG. 8. The potential difference is shown for the two inclusions. Two cases are shown: (i) the case corresponding to the perfect-conducting limit as obtained by setting $\epsilon_1/\epsilon_0 \to \infty$ or $\mu_1/\mu_0 \to \infty$ for either surfaces/metasurfaces and (ii) the case of a metasurface which gives the perfect-conducting result for the values here taken to be $\beta = (0.301)^2$, $\epsilon_0 = \mu_0 = 2.0$, $\epsilon_1 = \mu_1 = -3.6$, and $\epsilon_2 = \mu_2 = 3.0$. Remarkably, we see that we can reproduce the voltage between the inclusions for the perfect-conducting case via a metasurface design using finite valued parameters instead of the required infinite parameters needed in a right-handed medium. The two curves are exact and so lie on top of each other.

$$\frac{\Delta V}{V_0} = 2 - \gamma - 2\sum_{n=2}^{\infty} \left(\frac{n}{n+1}\right)\gamma^n \left[\prod_{k=1}^{n-1} \left(\frac{k}{k+1}\right)^2\right]. \tag{48}$$

Equation (48) is particularly easy to expand and can be truncated to a few orders N with excellent convergence hence avoiding the summation to infinity. Furthermore, for the special limit where the inclusions are perfect conducting, $\gamma = \gamma_{MG} = 1$; therefore, the sum in Eq. (48) reduces to the form

$$2\sum_{n=2}^{\infty} \left(\frac{n}{n+1}\right)\left[\prod_{k=1}^{n-1} \left(\frac{k}{k+1}\right)^2\right] = \sum_{n=2}^{\infty} \left[\frac{1}{n} - \frac{1}{n+1}\right]. \tag{49}$$

Equation (49) has the limit

$$\sum_{n=2}^{\infty} \left[\frac{1}{n} - \frac{1}{n+1}\right] = \frac{1}{2} - \frac{1}{3} + \frac{1}{3} - \frac{1}{4} + \frac{1}{4} + \cdots = \frac{1}{2} \tag{50}$$

so that Eq. (48) becomes

$$\frac{\Delta V}{V_0} = 2 - 1 - 2\frac{1}{2} \equiv 0 \tag{51}$$

for the case of perfect-conducting inclusions in contact. Equations (42) and (48) in particular determine the behavior of the inclusions at various separations including the limits of close interaction and touching. This is important for example for split-ring resonators since we require knowledge of how the capacitance of one SRR interacts with another and the medium itself or more generally what the coupling effects are. Figure 8 is a plot of the voltage between binary inclusions in the perfect-conducting limit $\gamma = 1$. This result applies both to inclusions inside surfaces and metasurfaces in the appropriate limit, and such behavior requires infinite val-

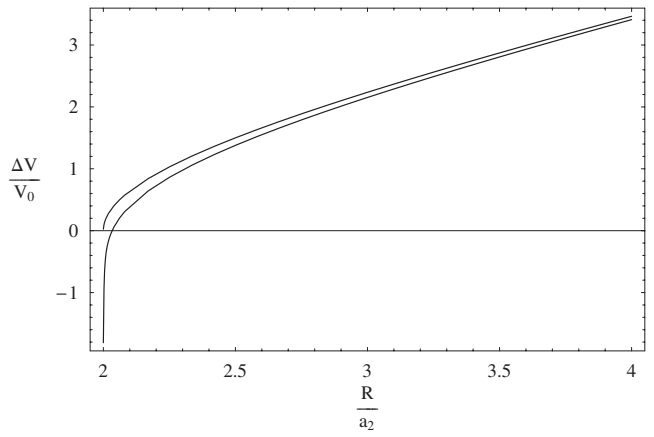

FIG. 9. The potential difference is shown for the two inclusions with the same parameters as in Fig. 8 except that now $\beta=(0.322)^2$. The curve that terminates at zero [predicted via Eq. (51)] is the same as that of Fig. 8 and is compared using the new β. In the latter case the voltage becomes negative as the two inclusion separations become infinitesimally small. This implies a negative capacitance effect.

ues for ϵ_1 and μ_1 which in practical terms may be a problem. However using the parameters shown in Fig. 8, for example, one sees that the perfect-conducting limit can also be attained via finite valued quantities. In Fig. 9, the perfect-conducting limit is shown using the same parameters as in Fig. 8 and then compared to the case where β is changed which results in a negative limit for closely packed inclusions. This characteristic for inclusions in a metasurface is possible because unlike right-handed material inclusions where Eq. (44) is bound to the interval $-1\leq\gamma\leq 1$ since

$$\lim_{\alpha\to 0}\ \gamma=-1 \quad \text{(holes limit)} \tag{52}$$

and

$$\lim_{\alpha\to\infty}\ \gamma=+1 \quad \text{(perfect-conducting limit)} \tag{53}$$

where $\alpha=\epsilon_1/\epsilon_0$, the filling fraction β for metasurface inclusions can make $\gamma>1$ and hence $\Delta V/V_0<0$. As $\gamma\gg 1$ we have $\Delta V/V_0\to-\infty$, or viewing this another way, the inner layer of the inclusion (filling fraction β) approaches that of the outer layer ($\beta\to 1$). This interesting phenomenon implies a negative capacitance which is a topic of debate for many researchers [28,29]. It would appear that the induced field of the inclusions is out of phase with the applied field with the former in fact being larger than the applied field $\mathbf{E}_0$ which explains the reason for the close proximity of SRRs in metamaterial design. The results derived here emphasize the enormous importance of modeling split-ring resonators as not just individual inclusions coupling with the medium but also in terms of coupling between each other as well. Such an analysis facilitates a more accurate understanding of the parameters involved in the development of negative permeability (μ) surfaces. Finally, the same approach can be used in the study of the voltage and capacitance between binary inclusions in a conventional right-handed surface if we make use of γ_{MG} instead of the metasurface analog γ.

V. DISCUSSION

There are many mean-field treatments of systems consisting of inclusions in a medium. Two well-known approaches are the Maxwell-Garnett and Bruggeman theories. In this paper we have made use of the former and expressed a way of incorporating many-body effects. However, like all mean-field treatments, the Maxwell-Garnett approach is not an exact theory. It takes into account single-particle interactions without self-consistency. On the other hand, Bruggeman's theory is self-consistent but overcorrects the two-body interaction terms. In this paper we have obtained the *exact* two-body interactions via a virial expansion in the area filling fraction. These results show to what extent the Maxwell-Garnett and Bruggeman theories fail at the second order; i.e., we gain knowledge of what discrepancy exists between the Maxwell-Garnett and Bruggeman methods by examining the correct two-body interaction terms. As far as the author is aware, there is no better way of testing the convergence properties of these two theories without extending to two or more particle interactions. The study of interacting binary particles is not new. In fact most of these studies involve three-dimensional (3D) spherical two-body interactions [30–37] starting from the classical paper by Jeffrey [38]. There have even been results reported for interacting binary cylinders that make use of cylindrical harmonics as basis functions in order to write the electric potential in terms of multipolar moments for the charge distribution in the cylinders [39]. However, generally speaking, the approaches used employ mathematical techniques that are too involved, e.g., spherical harmonics or asymptotics. Moreover these methods are also too complicated and inefficient for computational purposes. For example, using the multipole expansion method for two interacting spherical particles requires the inversion of a matrix consisting of hundreds of thousand of elements, depending on the required convergence. In addition, the full wave solution to the Helmholtz equation is generally nonseparable for spherical or disk inclusions. The alternative approach we have studied in this paper uses the method of images which allows us to obtain exact results for a 2D system and is computationally more efficient. For most practical calculations, Eqs. (23) and (24), for example, can be done analytically. The other important reason why we have obtained the two-body interaction terms via the method of images in a virial expansion is because, unlike other approaches, it allows a more direct way of summing up the series appearing in binary interactions and allows better manipulation of such results. Such a resummation for the two-body problem presented here might be useful in understanding or predicting many-body interactions. Another useful outcome of the approach we have used is that it gives incredible physical insight into how polarization effects build up order by order in an expansion involving particle separations. This is central to the idea of manipulating particle polarization and is applied to such areas as scattering cross-section reduction and cloaking [3,40–44]. The 2D theory presented in the paper can easily be extended to a 3D system consisting of spherical inclusions in a medium [45]. However, the results in 2D are exact because all we are required to do is determine the mapping distribution of point

dipoles between binary inclusions. For 3D systems, however, while the point-dipole contributions give excellent results for most problems, they do not give exact results. This is because for binary spherical particle interactions we require the mapping distribution of not just the point dipoles but also point charges as well as line dipole and line charge densities, respectively. It is possible to include the latter for 3D problems but the expressions obtained for the line densities in particular become mathematically too complicated to use without employing symbolic computations in high-end software such as MATHEMATICA or MATLAB which in turn means extensive use of memory and computational power. It is worth mentioning that in the superconducting limit for 3D binary particles the line densities vanish, thus simplifying the problem a little. Finally, the exact two-body approach presented has been used to obtain the effective permittivity and permeability of normal right-handed composite surfaces as well as for metasurfaces containing DNG inclusions. Using the approach farther, we have shown that it is possible to calculate the voltage between binary inclusions. Understanding of such interactions is necessary because among other things, in obtaining DNG surfaces, if inclusions are too close to each other DNG behavior is weak because the resonating interactions between the inclusions are too strong and "wash" out the effect of the negative permittivity and permeabilty and if the inclusions are too far apart there is no DNG effect.

VI. CONCLUSION

Conventional EMT has been extended to incorporate two-body interactions via the induced dipole moments between them. A general polarization factor has been used in the Maxwell-Garnett theory that allows both right-handed and left-handed composite surfaces to be studied. Negative and doubly negative metasurfaces are modeled in an effective-medium distribution and the potential difference (voltage, capacitance) of binary inclusions has been presented with a view to also analyze split-ring resonators. The results address the physics of surface/metasurface design more accurately than the conventional one-body EMT does. Ultimately the next step will be to include many-body interactions, but this is a very difficult task in view of the fact that even the three-body problem requires extremely complicated nonanalytic methods to solve it.

[1] V. G. Veselago, Sov. Phys. Usp. **10**, 509 (1968).
[2] J. B. Pendry, Phys. Rev. Lett. **85**, 3966 (2000).
[3] N. Engheta and R. W. Ziolkowski, IEEE Trans. Microwave Theory Tech. **53**, 1535 (2005).
[4] D. R. Smith, W. J. Padilla, D. C. Vier, S. C. Nemat-Nasser, and S. Schultz, Phys. Rev. Lett. **84**, 4184 (2000).
[5] T. A. Klar, A. V. Kildishev, V. P. Drachev, and V. M. Shalaev, IEEE J. Sel. Top. Quantum Electron. **12**, 1106 (2006).
[6] V. M. Agranovich, Y. R. Shen, R. H. Baughman, and A. A. Zakhidov, Phys. Rev. B **69**, 165112 (2004).
[7] J. B. Pendry, D. Schurig, and D. R. Smith, Science **312**, 1780 (2006).
[8] A. Sihvola, PIER **66**, 191 (2006).
[9] J. Han, Opt. Express **16**, 1354 (2008).
[10] O. Acher, J.-H. Le Gallou, and M. Lediou, Metamaterials **2**, 18 (2008).
[11] A. Boltasseva and V. M. Shalaev, Metamaterials **2**, 1 (2008).
[12] W. M. Klein, C. Enkrich, M. Wegener, C. M. Soukoulis, and S. Linden, Opt. Lett. **31**, 1259 (2006).
[13] H. A. Lorentz, *Theory of Electrons* (Dover, New York, 1952).
[14] R. Landau, *Electrical Conductivity in Inhomogeneous Media-Electrical Transport and Optical Properties of Inhomogeneous Media*, AIP Conference Proceedings No. 40, Ohio State University, 1977 (AIP, New York, 1978), pp. 2–45.
[15] See W. Thompson, *Reprint of Paper on Electrostatics and Magnetism*, 2nd ed. (Macmillan, London, 1848), pp. 52–85.
[16] J. C. Maxwell, *Electricity and Magnetism*, 1st ed. (Clarendon, Oxford, 1873).
[17] B. R. Djordjević, J. H. Hetherington, and M. F. Thorpe, Phys. Rev. B **53**, 14862 (1996).
[18] T. C. Choy, *Effective Medium Theory: Principles and Applications* (Clarendon, Oxford, 1999).
[19] A. Alexopoulos, J. Phys. A **37**, 11911 (2004).
[20] A. Alexopoulos, Phys. Lett. A **338**, 385 (2005).
[21] J. Pendry, A. J. Holden, D. D. Robbins, and W. J. Stewart, IEEE Trans. Microwave Theory Tech. **47**, 2075 (1999).
[22] J. E. Page, J. Esteban, and C. Camacho-Peñalosa, AEU, Int. J. Electron. Commun. **63**, 327 (2009).
[23] L. D. Landau and E. M. Lifshitz, *Electrodynamics of Continuous Media* (Pergamon, Oxford, 1960), p. 251.
[24] R. Merlin, Proc. Natl. Acad. Sci. U.S.A. **106**, 1693 (2009).
[25] D. J. Cho, F. Wang, X. Zhang, and Y. R. Shen, Phys. Rev. B **78**, 121101(R) (2008).
[26] V. M. Agranovich and Yu. N. Gartstein, Phys. Usp. **49**, 1029 (2006).
[27] V. M. Agranovich and Yu. N. Gartstein, Metamaterials **3**, 1 (2009).
[28] E. Ershov, H. C. Liu, L. Li, M. Buchanan, Z. R. Wasilewski, and A. K. Jonscher, IEEE Trans. Electron Devices **45**, 2196 (1998).
[29] Y. Okawa, H. Norimatsu, H. Suto, and M. Takayanagi, in *International Conference on Microelectronic Test Structures* (IEEE, Piscataway, NJ, 2003), pp. 197–202.
[30] F. Claro and R. Fuchs, Phys. Rev. B **33**, 7956 (1986).
[31] R. G. Barrera, G. Monsivais, and W. L. Mochán, Phys. Rev. B **38**, 5371 (1988).
[32] B. U. Felderhof and R. B. Jones, Phys. Rev. B **39**, 5669 (1989).
[33] F. Claro and R. Rojas, Phys. Rev. B **43**, 6369 (1991).
[34] K. Hinsen and B. U. Felderhof, Phys. Rev. B **46**, 12955 (1992).
[35] R. G. Barrera, J. Giraldo, and W. L. Mochán, Phys. Rev. B **47**, 8528 (1993).
[36] B. Cichocki and B. U. Felderhof, J. Chem. Phys. **107**, 6390

(1997).
[37] C. Tserkezis, G. Gantzounis, and N. Stefanou, J. Phys.: Condens. Matter **20**, 075232 (2008).
[38] D. J. Jeffrey, Proc. R. Soc. London, Ser. A **335**, 355 (1973).
[39] R. Rojas, F. Claro, and C. R. Proetto, Phys. Rev. E **62**, 5688 (2000).
[40] A. Alù and N. Engheta, Phys. Rev. E **72**, 016623 (2005).
[41] M. Silveirinha, A. Alù, and N. Engheta, Phys. Rev. E **75**, 036603 (2007).
[42] A. Alù and N. Engheta, Opt. Express **15**, 3318 (2007).
[43] A. Alù and N. Engheta, Opt. Express **15**, 7578 (2007).
[44] A. Alù and N. Engheta, Phys. Rev. Lett. **100**, 113901 (2008).
[45] A. Alexopoulos, Phys. Lett. A **373**, 3190 (2009).